

Holistic atlases of functional networks and interactions (HAFNI) 15

X. Jiang¹, D. Zhu², T. Liu¹

The University of Georgia, Athens, GA, United States¹ University of Southern California,
Los Angeles, CA, United States²

CHAPTER OUTLINE

15.1 Introduction	435
15.2 HAFNI for Functional Brain Network Identification	439
15.3 HAFNI Applications	442
15.4 HAFNI-Based New Methods	449
15.5 Future Directions of HAFNI Applications	451
Acknowledgments	451
References	451

15.1 INTRODUCTION

An unrelenting human quest in neuroscience is to understand the organizational architecture of brain function, which to a great extent defines what we are and who we are. After decades of active research, functional magnetic resonance imaging (fMRI) (Biswal et al., 1995; Ogawa et al., 1990a,b) became a popular neuroimaging technique due to its noninvasive and *in vivo* nature. For example, blood oxygenation level-dependent (BOLD) contrast (Ogawa et al., 1990a,b), a commonly used form of fMRI, can detect local changes in deoxyhemoglobin concentration and is believed to represent a vascular coupling from neuronal activities. In general, fMRI aims to explore the brain's functional activities by leveraging the relations between brain neural activity and hemodynamics (Friston, 2009; Logothetis, 2008). Since its inception in 1990 (Ogawa et al., 1990a,b), modern fMRI techniques have been applied widely and have become the most important way to study brain functions (Friston, 2009; Logothetis, 2008) in the past decade. In particular, task fMRI (tfMRI) has been commonly adopted as a benchmark approach in mapping and localizing

functionally specialized brain areas under specific task stimulus (Friston, 2009; Logothetis, 2008). Meanwhile, resting state fMRI (rsfMRI) has been increasingly applied to explore and map intrinsic connectivity networks (ICNs) based on the fact that correlated brain activity patterns have been reported to have similar low-frequency oscillations within rsfMRI time series (Cohen et al., 2008; Fox and Raichle, 2007; Van Den Heuvel et al., 2008).

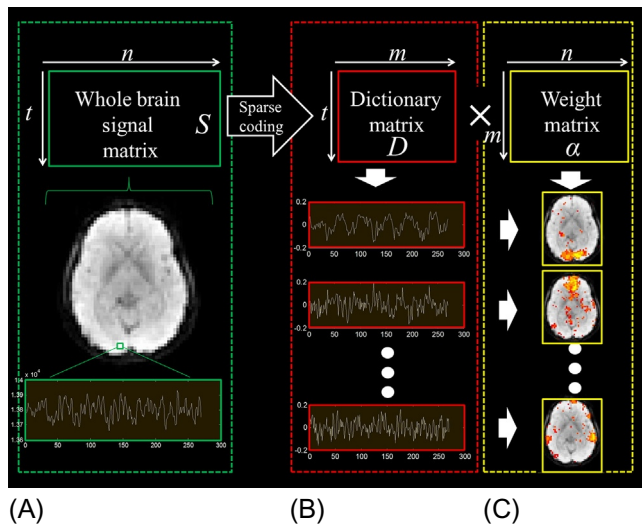
In the computational neuroscience community, a variety of computational and statistical methods targeting fMRI BOLD signals analysis have been developed for activation detection and latent functional network modeling, such as correlation analysis (Bandettini et al., 1993), principal component analysis (PCA) (Anderson et al., 1999), general linear model (GLM) (Friston et al., 1994; Worsley, 1997), Markov random field (MRF) models (Descombes et al., 1998), independent component analysis (ICA) (McKeown et al., 1998, 2003; Calhoun and Adali, 2006), mixture models (Hartvig and Jensen, 2000), autoregressive spatial models (Woolrich et al., 2001), wavelet algorithms (Bullmore et al., 2003; Shimizu et al., 2004), empirical mean curve decomposition (Deng et al., 2012), and Bayesian approaches (DuBois Bowman et al., 2008). Of all these methods, GLM and ICA are the most widely used methods for tfMRI and rsfMRI, due to their effectiveness, robustness, simplicity, and wide availability. GLM considers the relationship of observed data and given factors: As a linear model, the observations or responses are formed as a linear combination of a series of known factors. For tfMRI, the external stimulus can be used to construct the regressors (design matrix) by convolution with hemodynamic response function (hrf) (Wagenmakers, 2015). The outcome of GLM analysis is a statistic (eg, z score) for each voxel, which indicates if the response of that voxel is task-related. For rsfMRI, model-free approaches (like ICA) are widely accepted since, given that there is no external stimulus, it is difficult to infer or design a model which can effectively interpret resting-state BOLD fluctuations. In essence, ICA is based on matrix factorization and its objective function is to maximize the statistical independence (eg, minimize the mutual information) between any pair of components. ICA-based methods aim to explore a mixture of underlying sources that can explain the brain activity patterns in the resting state (van den Heuvel and Pol, 2010).

Despite the significant neuroscientific insights and remarkable successes of the above-mentioned methods in the past decades, we are still facing challenges as our understanding becomes deeper regarding the organization of brain architecture. For example, it has been pointed out that spatially overlapping networks subserving different brain functions may be unnoticed by the traditional blocked subtraction paradigms and the related analysis methods, such as GLM (Krekelberg et al., 2006; Logothetis, 2008). It also has been widely argued that a variety of cortical areas and brain networks exhibit remarkable functional diversity and heterogeneity (Anderson et al., 2013; Duncan, 2010; Fedorenko et al., 2013; Kanwisher, 2010; Pessoa, 2012). That is, the human brain is widely considered as containing a collection of highly specialized functional networks, which are able to flexibly interact with

each other when distinct brain functions are performed. In such a scenario, activity in one brain region might need to recruit multiple neuroanatomical regions in a temporal sequence. Meanwhile, the same brain area might also participate in multiple functional processes simultaneously with different internal or external circumstances. As a consequence, the corresponding fMRI BOLD signal from a single voxel tends to be composed of various components corresponding to multiple functional sources. Therefore traditional subtraction-based tfMRI analysis methods (eg, GLM) might be insufficient to reconstruct all or most concurrent spatially and temporally overlapping brain functional networks. Indeed, ICA and its variations, such as spatial ICA and temporal ICA, perform better than GLM in the identification of concurrent functional components (eg, ICNs). Nevertheless, given the fact that we still have very limited understanding about the exact mechanism of the brain's functional operations, we might need to carefully consider the rationale and validity of applying any preset assumptions, like statistical independence in ICA.

In our opinion, an ideal solution to fMRI data analysis should have at least the following characteristics: (1) it should consider the complexity of fMRI BOLD signals which arise from different signal sources including the interactions of multiple activated functional networks; (2) it should conform to the neuroscience principle that multiple functional networks can be activated simultaneously and they might interact with each other; (3) it should impose as few assumptions as possible. As an attempt to better understand and interpret fMRI BOLD time series, in the following part of this chapter, we introduce a novel machine learning-based alternative methodology, called *holistic atlases of functional networks and interactions* (HAFNI), which employs a sparse representation of whole-brain fMRI signals for functional network identification in both tfMRI and rsfMRI data (Lv et al., 2015b). The basic idea is that we aggregate hundreds of thousands of tfMRI or rsfMRI signals within the whole brain from a single subject into a big data matrix (represented as S in Fig. 15.1A), and factorize it by an over-complete dictionary basis matrix (represented as D in Fig. 15.1B) and a sparse reference weight matrix (represented as α in Fig. 15.1C) via an effective online dictionary learning algorithm (Mairal et al., 2010). The derived time series in the learned basis dictionary represent different activities of concurrent brain functional networks (the white curves in Fig. 15.1B). Their corresponding weight vectors (each row of α) stand for the spatial maps of these concurrent functional networks (the 3D volume images in Fig. 15.1C). One important characteristic of this framework is that the decomposed weight matrix naturally reflects the spatial overlap/interaction patterns of reconstructed brain networks (Lv et al., 2015b).

The advantages of HAFNI include: (1) Sparse representation naturally accounts for the complexity of BOLD signals in that each single fMRI time series is represented as a linear combination of common “blocks,” called dictionary atoms, which can correspond to different signal sources. Each dictionary atom also contributes to multiple fMRI signals simultaneously and the proportion of each contribution is

**FIG. 15.1**

The computational framework of sparse representation of whole-brain fMRI signals (from single brain) using online dictionary learning. (A) The whole-brain fMRI signals are integrated into a big data matrix, in which each row represents the whole-brain fMRI BOLD data at one time point and each column stands for the time series of a single voxel (green rectangle). (B) Illustration of the learned dictionary. Each column represents a latent functional network. Three exemplar dictionary atoms are shown in the bottom panels. (C) The decomposed sparse reference weight matrix. Each row contains the weight parameters of the corresponding functional network component.

encoded in the weight matrix. There is extensive literature suggesting that, through sparse learning, certain task-evoked and intrinsic connectivity networks (ICNs) can be successfully recovered (Varoquaux et al., 2013). (2) Based on the learned dictionary atoms, we are able to identify latent functional networks, especially those corresponding to external stimulus (designed tasks) or ICNs (eg, default mode network, DMN), which influence the behavior of the brain in a temporal sequence. (3) Unlike ICA, we do not enforce any predefined constraints except sparsity of the weight matrix. However, sparsity reflects a widely accepted precondition of how the brain works: only parts of the brain are involved in performing a task at one time. In the rest of this chapter, we will first discuss the results after applying HAFNI to the publicly released large-scale Human Connectome Project (HCP) high-quality fMRI data (Section 15.2), which is followed by three applications of HAFNI, including clinical studies, cerebral cortex structural/functional architecture exploration, and neuroimaging-informed multimedia analysis (Section 15.3). Then we will consider some new HAFNI-based machine learning methods (Section 15.4) and provide insights into the future directions of HAFNI (Section 15.5).

15.2 HAFNI FOR FUNCTIONAL BRAIN NETWORK IDENTIFICATION

We have applied HAFNI to the Q1 release of the HCP tfMRI dataset, which includes seven tasks (motor—M, emotion—E, gambling—G, language—L, relational—R, social—S, and working memory—WM) for 77 participants. More details of demographics, preprocessing, and data acquisition can be found in [Smith et al. \(2013\)](#). In total, we have identified and confirmed 23 group-wise consistent task-evoked networks, called task-evoked HAFNI components, for motor (M1–M5 in [Fig. 15.2A](#)), emotion (E1–E3 in [Fig. 15.2A](#)), gambling (G1 and G2 in [Fig. 15.2A](#)), language (L1 and L2 in [Fig. 15.2A](#)), relational (R1 and R2 in [Fig. 15.2B](#)), social (S1–S3 in [Fig. 15.2B](#)), and working memory (WM) (W1–W6 in [Fig. 15.2B](#)) networks. The details of the identification of these 23 HAFNI networks can be found in [Lv et al. \(2015b\)](#). In addition, these HAFNI networks correspond to some specific task stimuli (see [Table 15.1](#)).

In particular, these 23 task-evoked HAFNI components are consistent and can be reproduced across all of the HCP subjects of the Q1 release ([Lv et al., 2015b](#)). In [Fig. 15.2A](#) and B, the averaged spatial maps of each HAFNI network across all

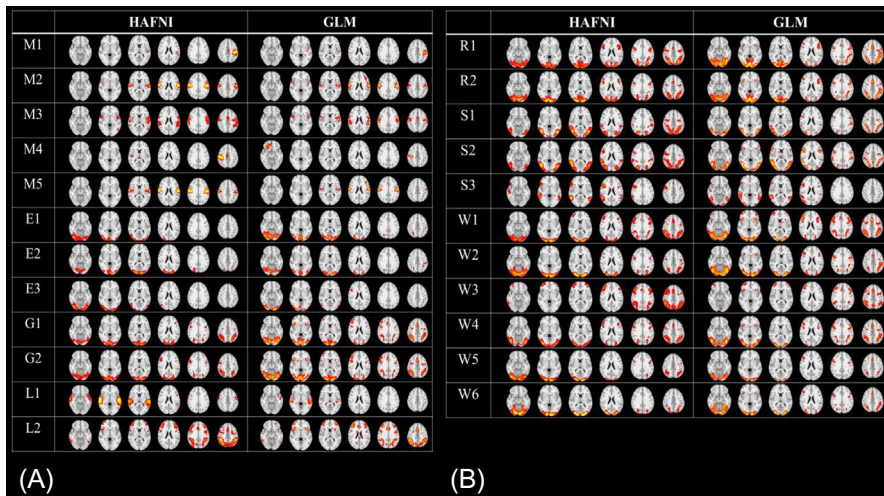


FIG. 15.2

The task-evoked HAFNI networks and the comparison with GLM-derived activation maps. The seven tasks are motor network (M), emotion network (E), gambling network (G), language network (L), relational network (R), social network (S), and working memory network (WM). (A, B) Group-wise averages of 23 identified HAFNI networks across all HCP subjects for the four tasks as well as the corresponding averaged GLM-derived activation maps (right column). Six representative volume slices are selected for visualization for each component.

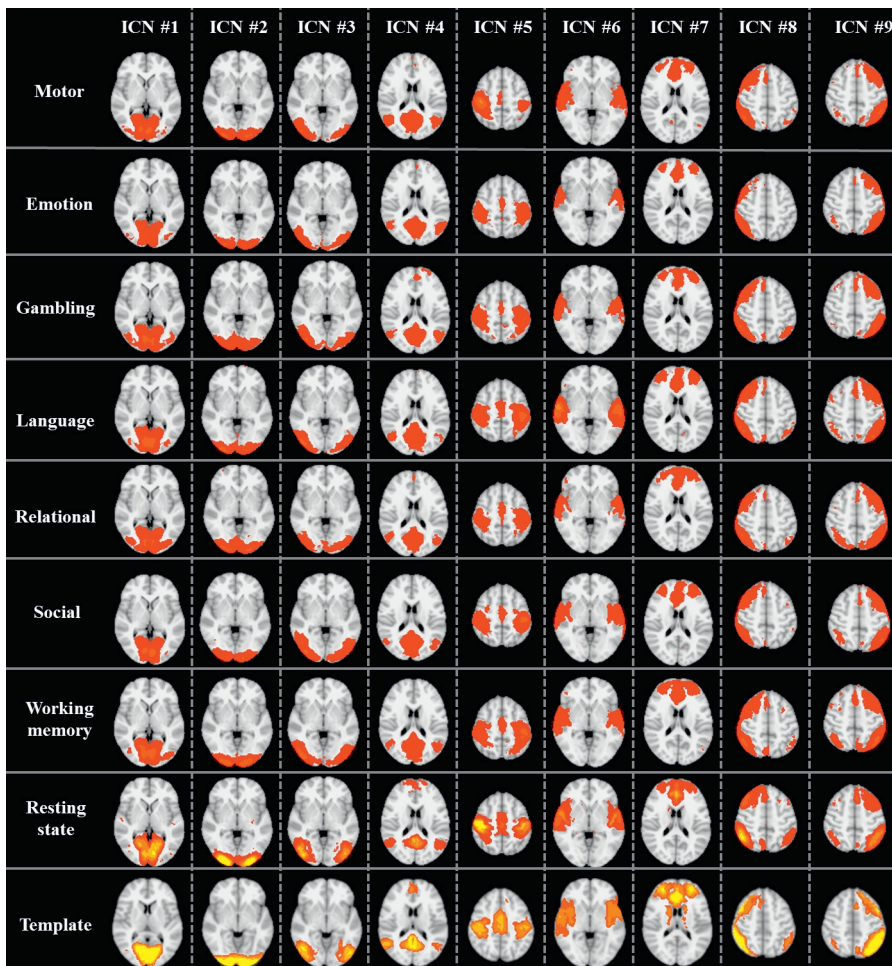
Table 15.1 Task Names of Task-Evoked HAFNI Components

HAFNI Component	Task Name	HAFNI Component	Task Name
M1	Right hand movement	R1	Match task
M2	Tongue movement	R2	Relational task
M3	Global motion	S1	Interaction behavior
M4	Left hand movement (over average)	S2	Random behavior
M5	Tongue movement (over average)	S3	Interaction over random
E1	Emotional faces	W1	2-back memory task
E2	Simple shapes	W2	0-back memory task
E3	Emotional faces over simple shapes	W3	2-back over 0-back
G1	Punishment	W4	Body part memorization
G2	Reward	W5	Face recognition
L1	Story	W6	Place recognition
L2	Math over story		

subjects are shown and compared to the group-wise GLM-derived activation map. We can see that the averaged HAFNI networks are similar to the group-wise GLM-derived maps. Note that all HAFNI networks are learned simultaneously from the optimally decomposed fMRI time series by sparse representation of whole-brain data (see Fig. 15.1). The GLM maps, however, are obtained from individual fMRI time series with separate model-driven subtraction procedures. For example, the five motor networks (M1–M5 in Fig. 15.2A) can be robustly identified by characterizing the most relevant atoms from a collection of candidate dictionary atoms, which can maximally interpret the whole-brain fMRI time series. On the contrary, GLM examines fMRI signals whose compositions can only arise from predefined activation models. As a consequence, GLM has difficulty in identifying latent and concurrent functional networks. In this situation, some spatially overlapping networks with distinct temporal curves such as ICNs (Fig. 15.3) in task data, other than the task paradigm, will be essentially ignored (Krekelberg et al., 2006; Logothetis, 2008).

HAFNI is also effective and efficient in reconstructing concurrent ICNs based on either tfMRI or rsfMRI data. Once the HAFNI framework is applied to the whole-brain tfMRI or rsfMRI signals for each individual subject, both quantitative measurement and visual inspection of the spatial pattern of dictionary atoms (functional networks) are integrated to identify and characterize the ICNs using existing brain science knowledge (Lv et al., 2015b). Specifically, the well-defined ICN templates provided in the literature (eg, Smith et al., 2009) are adopted as the references. We define the spatial similarity as the spatial overlap rate R between a dictionary atom's spatial pattern (S) and an ICN template (T) (Jiang et al., 2015; Lv et al., 2015b):

$$R(S, T) = \frac{|S \cap T|}{|T|}. \quad (15.1)$$

**FIG. 15.3**

The identified spatial patterns (averaged) of ICNs across all individual subjects in the seven tfMRI (motor, emotion, gambling, language, relational, social, and working memory) and one rsfMRI datasets in HCP Q1. The most informative slice superimposed on the MNI152 template image is visualized in each part. The color scale of the spatial pattern of ICNs ranges from 0.2 to 10 in the seven tfMRI data, and from 0.5 to 10 in rsfMRI data ([Lv et al., 2015b](#)).

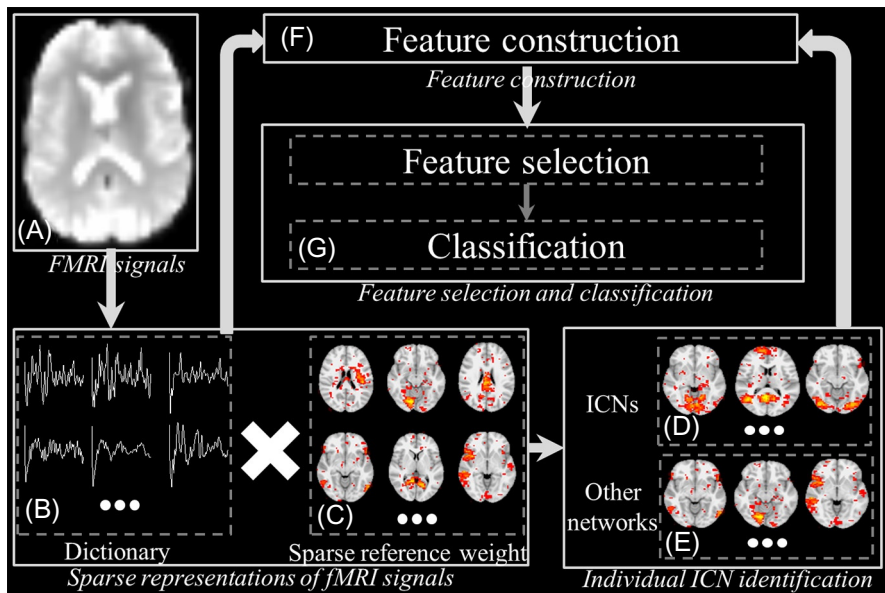
Note that S and T are converted from continuous values to discrete labels (all values less than or equal to 0 are labeled as 0, and others are labeled as 1). For the tfMRI or rsfMRI data of each subject, the dictionary atom with the highest spatial overlap rate to a specific ICN template (Eq. 15.1) is identified as the candidate of the

ICNs. A group of experts then quantitatively (spatial overlap rate) and qualitatively (visual inspection) examine the identified corresponding ICN candidates across a group of subjects. If all of the identified ICN candidates have high spatial overlap rate across all subjects, these dictionary atoms will be regarded as the identified ICNs for each subject. For example, in Lv et al. (2015a), the default mode network (DMN), which is a well known and interpreted ICN, was successfully identified in two tfMRI datasets (working memory and semantic decision making). In Lv et al. (2015b), nine ICNs were identified in the seven tfMRI and one rsfMRI datasets in the HCP Q1 release (Van Essen, 2013). Fig. 15.3 shows the averaged identified ICNs across all subjects in the seven tfMRI and one rsfMRI datasets. Specifically, ICNs 1–3 are located in the visual cortex. ICN 4 is in the DMN. ICNs 5–7 are the sensorimotor, auditory, and executive control networks respectively. ICNs 8–9 contain the frontal and parietal areas and have strong lateralization.

Based on the identified ICNs and task-evoked networks via HAFNI, we found significant spatial overlaps within task-evoked networks, within ICNs, and between task-evoked networks and ICNs (Lv et al., 2015a; Lv et al., 2015b), which may shed light on the exploration of the interaction among functional networks (both task-evoked networks and ICNs) to jointly fulfill brain function in the future (Lv et al., 2015b).

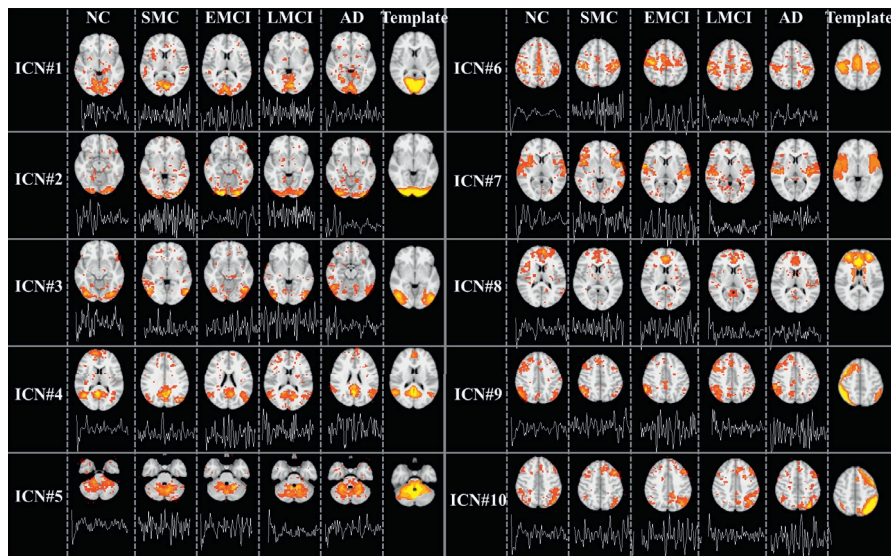
15.3 HAFNI APPLICATIONS

The HAFNI framework has gained increasing interest in a variety of applications. Here we briefly introduce three categories of applications. The first category is in clinical studies. For example, in our recent work (Jiang et al., 2014), the HAFNI framework was applied to the publicly available Alzheimer’s Disease Neuroimaging Initiative (ADNI) rsfMRI datasets. Alzheimer’s disease (AD) is one of the most common types of dementia and a major cause of death for elderly people (65 or older) (Thies and Bleiler, 2013). However, there is still no effective treatment for AD (Thies and Bleiler, 2013). Meanwhile, it has been demonstrated that the pre-stages of AD (including late mild cognitive impairment (LMCI), early mild cognitive impairment (EMCI), and significant memory concern (SMC)) have the potential to predict the conversion of AD or other neurodegenerative diseases (Petersen et al., 2001). Therefore effective and efficient classification of AD and its pre-stages as distinct from healthy people has received increasing interest. As illustrated in Fig. 15.4, the core idea in Jiang et al. (2014) is to identify the concurrent intrinsic functional networks including ICNs based on the HAFNI framework in five populations (normal control (NC), SMC, EMCI, LMCI, and AD groups), and to adopt meaningful features derived from those identified intrinsic functional networks to classify each of the four diseased groups from the NC group. Firstly, we identify 10 meaningful ICNs for each of the subjects based on the 10 ICN templates (Smith et al., 2009) via the HAFNI framework, as detailed in Section 15.2. Fig. 15.5 shows the 10 identified ICNs in one example subject brain of each of the five populations. ICNs 1–3 are located in

**FIG. 15.4**

Computational framework for discrimination of Alzheimer's disease (AD) and its pre-stages from healthy people based on the HAFNI framework. (A) Whole-brain rsfMRI data of an individual subject. (B) Dictionary matrix. (C) Sparse reference weight matrix. (D) Ten identified ICNs based on ICN templates. (E) Other dictionary atoms. (F) Six types of features constructed based on the dictionary matrix and identified ICNs. (G) Correlation-based feature selection (CFS) and support vector machine (SVM) classifier based classification between a diseased group and normal control group.

the visual cortex. ICNs 4–8 are in the DMN, cerebellum, sensorimotor, auditory, and executive control networks respectively. ICNs 9–10 are located in the frontal and parietal areas and have strong lateralization. Secondly, we construct a collection of meaningful features based on the dictionary matrix and identified intrinsic functional networks. Specifically, six types of features which can efficiently and effectively represent both spatial and functional characteristics of brains during the resting state are constructed for each subject (Jiang et al., 2014). The first type of feature is the spatial overlap rate R between an identified ICN and the corresponding ICN template as defined in Eq. (15.1). The second type is the functional connectivity within ICNs. We calculate the Pearson correlation value between any pair of temporal patterns of the 10 ICNs to obtain a 10 by 10 symmetric matrix, and adopt its 45 unique elements as the features. The third type is the functional connectivity within all dictionary components. Besides the connectivity within ICNs in the third type, we also examine the functional connectivity between the ICNs and the other functional

**FIG. 15.5**

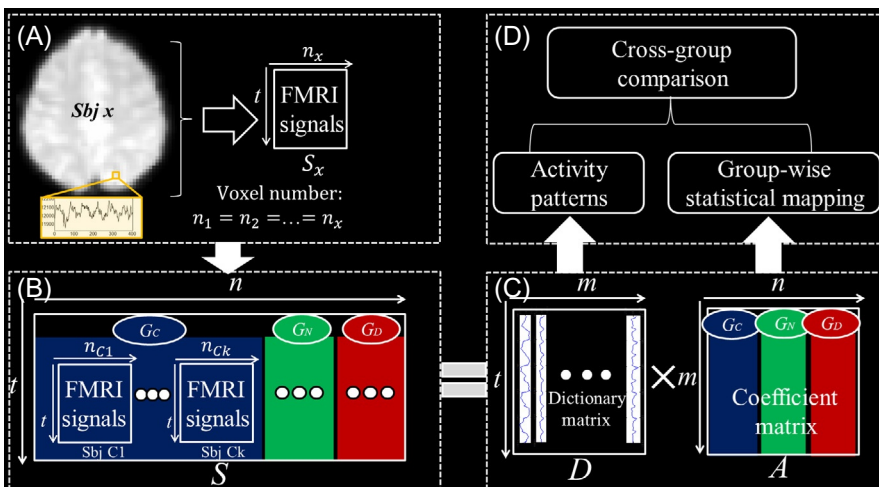
Ten identified ICNs based on HAFNI in one example subject brain of each of the five population groups. Each part shows the most informative slice, which is superimposed on the MNI152 template image and the temporal pattern of the corresponding dictionary atom. The color scale of each part ranges from 0.1 to 10. The 10 ICN templates (thresholded at $z = 3$) are provided in [Smith et al. \(2009\)](#).

components. The second and third types of feature are complementary since they represent the functional connectivities between dictionary components from different perspectives. Instead of the traditional functional connectivity measurement based on raw fMRI signals, we measure the functional connectivity based on the temporal patterns of dictionary atoms, which reflect the intrinsic functional activities of brain networks. The fourth type is the entropy of functional connectivity. We construct a histogram which represents the functional connectivity distribution based on the third type of feature. Twenty equal-distance bins are adopted to cover $[-1, +1]$ and the Shannon entropy is calculated. The fifth type of feature is the entropy of component distribution within ICNs. For each voxel involved in an ICN component, we count the dictionary atoms which are involved when representing the original rsfMRI signals to obtain a distribution histogram of the number of voxels involved in each dictionary, and calculate the Shannon entropy of the distribution histogram as the feature. The sixth type of feature is the common dictionary distribution. Based on the dictionary matrix obtained for each subject, we perform second-round dictionary learning and sparse coding on the dictionaries in order to obtain the common dictionary atoms among all atoms. We then obtain the distribution of the number of individual dictionary atoms which can be represented by each common dictionary

Table 15.2 The Classification Accuracy for Each Group Pair

	NC-SMC (%)	NC-EMCI (%)	NC-LMCI (%)	NC-EMCI+LMCI (%)	NC-AD (%)
Accuracy	92.31	80.00	80.68	92.00	94.12
Specificity	96.15	76.00	79.55	90.00	94.12
Sensitivity	88.46	84.00	81.82	94.00	94.12

atom as the sixth type of feature. Thirdly, in order to preserve only those features with most differentiation power, we perform feature selection on all six types of features via correlation-based feature selection (CFS) (Hall and Smith, 1999). Then the support vector machine (SVM) classifier (Chang and Lin, 2011) is performed on the discriminative features for classification between each diseased group and the normal control group respectively. The experimental results indicate that the HAFNI-based computational framework achieves high discriminative accuracy for AD and its pre-stages from normal control, as detailed in **Table 15.2**.

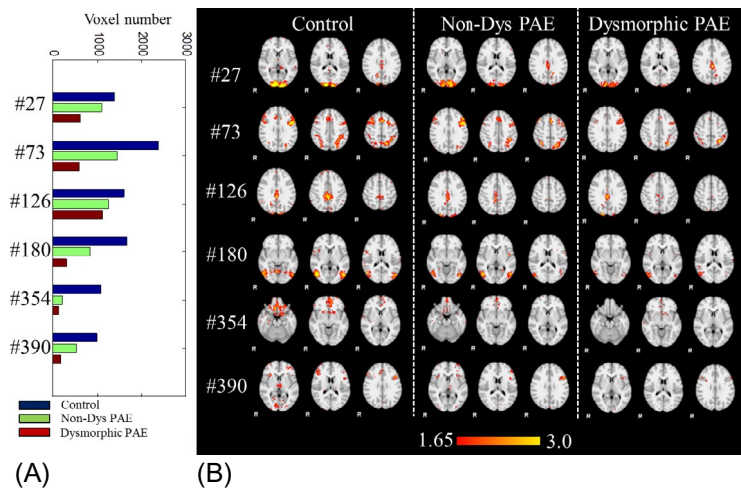
**FIG. 15.6**

The computational framework of group-wise sparse representation of fMRI signals for identification of affected functional networks among healthy control, nondysmorphic PAE, and dysmorphic PAE groups. (A) Aggregated signal matrix of one single subject. (B) Aggregated large signal matrix S from all signal matrices of the three groups of subjects. G_C , healthy control group; G_N , nondysmorphic PAE group; G_D , dysmorphic PAE group. t is the fMRI time point. (C) The learned dictionary matrix D and the sparse reference weight matrix A . A is decomposed into multiple submatrices corresponding to the sparse reference weight matrix of each subject. (D) Cross-group comparison is performed based on D and A .

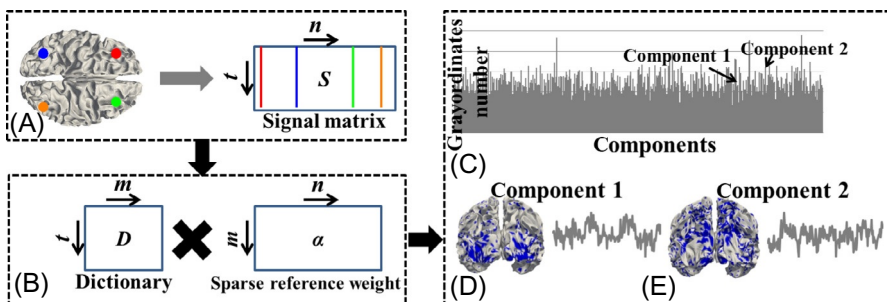
Another example of HAFNI-based application in clinical studies is to identify possible functional abnormalities among healthy control, exposed nondysmorphic prenatal alcohol exposure (nondysmorphic PAE), and exposed dysmorphic prenatal alcohol exposure (dysmorphic PAE) groups using the HAFNI-based group-wise sparse coding framework (Lv et al., 2015c). As illustrated in Fig. 15.6, firstly, the whole-brain tfMRI signals of each subject are extracted and aggregated into a signal matrix. Secondly, the signal matrices of all three groups of subjects (healthy control, nondysmorphic PAE, and dysmorphic PAE) are arranged into a large signal matrix S . Thirdly, the dictionary learning and sparse coding framework is applied on S to learn a common dictionary D and a sparse reference weight matrix A . Since the sparse reference weight matrix A preserves the organization of subjects and groups in S , it is decomposed into multiple submatrices corresponding to the sparse reference weight matrix of each subject. Finally, cross-group comparisons are performed based on the multiple submatrices and those brain functional networks/regions which are affected by nondysmorphic PAE or dysmorphic PAE can be assessed. Experimental results show that the proposed approach effectively identifies a collection of brain networks/regions that are affected by nondysmorphic PAE or dysmorphic PAE group. Fig. 15.7 illustrates the six dominant networks of which the size (number of voxels involved in the network) decreases with the increment of severity of PAE. Specifically, networks 27, 126, and 180 (the indexes of networks are referred to in Lv et al., 2015c) belong to diverse dynamic networks, networks 73 and 390 are task-evoked networks, and network 354 is an antitask network (Lv et al., 2015c). We can see that for each of the six networks, the size is largest in the control group, smallest in the dysmorphic PAE group, and moderate in the nondysmorphic PAE group. The decreased regions include the visual cortex and default mode network for diverse dynamic networks, left superior and right inferior parietal regions and medial frontal gyrus for task-evoked networks, and subcortical regions and medial prefrontal cortex for the antitask network.

The second category of HAFNI applications is computational modeling of cerebral cortex structural/functional architecture. The human cerebral cortex is composed of highly convoluted cortical folding, including convex gyri and concave sulci (Rakic, 1988). To explore the possible functional difference between cortical gyri and sulci, Jiang et al. (2015) applied the HAFNI framework on the HCP gray-ordinate tfMRI data to identify both task-evoked networks and ICNs, to systematically characterize task-based heterogeneous functional regions (THFRs) on the cortical surface (the regions that are involved in multiple task conditions when performing a specific task), and to assess the spatial patterns of those task-based heterogeneous functional regions on cortical gyri and sulci. Specifically, both meaningful task-evoked networks and ICNs are firstly identified for each subject in each task based on HAFNI, as detailed in Section 15.2 and illustrated in Fig. 15.8. Secondly, we define THFR by assessing the number of involved functional networks (dictionary components) of each gray-ordinate g_i ($i = 1, \dots, n$, n is the number of gray-ordinates):

$$\text{THFR} = \forall g_i \text{ s.t. } \|\alpha_i\|_0 > q, \quad (15.2)$$

**FIG. 15.7**

Six dominant networks of which the size (number of voxels involved in the network) decreases with the increment of severity of PAE, that is, $V(\text{Control}) > V(\text{Non-Dys PAE}) > V(\text{Dysmorphic PAE})$. (A) Comparison of voxel numbers ($P < 0.05$, $Z > 1.65$) involved in the six networks among the three groups. (B) Comparison of the spatial pattern (z-score map) of the six networks among the three groups. The indexes of networks are referred to in Lv et al. (2015c).

**FIG. 15.8**

Computational framework of sparse representation of gray-ordinate-based fMRI signals based on HAFNI. (A) Aggregated signal matrix S of one example subject. Four example cortical vertices (gray-ordinates) and associated signals are represented by four different colors (red, blue, green and orange) (four gray dots in print versions). t is the fMRI time point and n is the gray-ordinate. (B) Learned dictionary matrix D and sparse reference weight matrix α . m is the number of dictionary components. (C) The distribution histogram of the number of gray-ordinates involved in each dictionary component. (D, E) The spatial pattern on the cortical surface (highlighted by blue) (gray in print versions) and temporal pattern (gray curve) (gray in print versions) of two example dictionary components respectively.

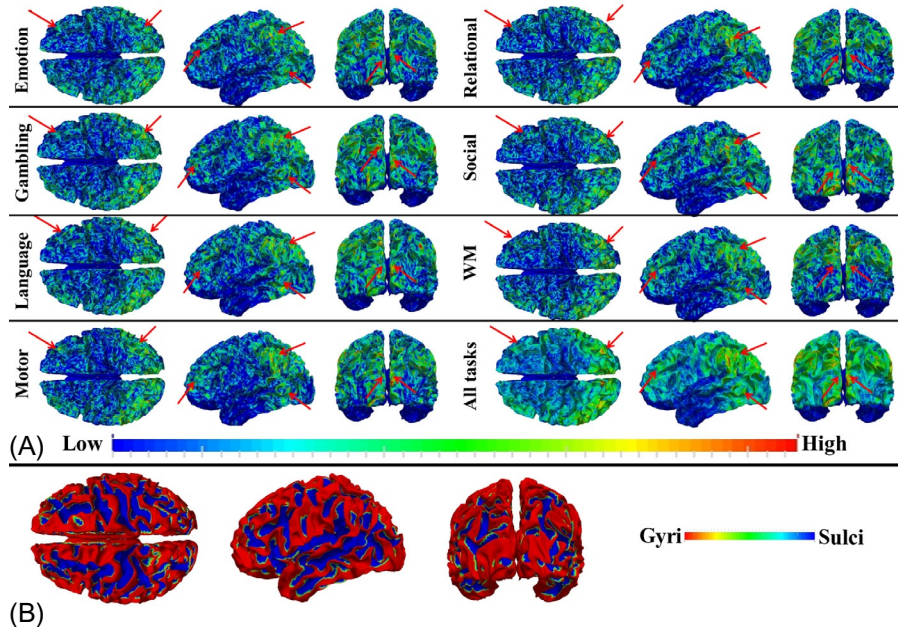


FIG. 15.9

(A) Spatial distribution density map of identified THFRs across all subjects in each of the seven tfMRI data sets (emotion, gambling, language, motor, relational, social, and working memory (WM)) and across all seven tfMRI data sets shown on one example subject. The THFRs which are relatively consistent across seven tasks and with higher distribution density are highlighted by red arrows (gray in print versions). (B) The gyri/sulci regions of the example subject.

where α_i is the i th column of α representing the functional network composition of g_i THFR is a collection of gray-ordinates of which the involved functional networks (number of nonzero elements in α_i) is larger than a threshold q (Jiang et al., 2015). Fig. 15.9 shows the spatial distribution density map of identified THFRs across all subjects in each of the seven tfMRI data sets. We can see that the THFRs are mainly located at the bilateral parietal lobe, frontal lobe, and visual association cortices. We further assess the distribution percentage of the THFRs on cortical gyral and sulcal regions respectively. Experimental results demonstrate that THFRs are located significantly more on gyri than on sulci across all seven tasks, as reported in Table 15.3. The proposed HAFNI-based framework for identification of THFRs indicates the functional difference between gyri and sulci during task performance, and might advance the understanding of the exact functional mechanisms of human cerebral cortex in the future (Jiang et al., 2015).

The third category of HAFNI applications is neuroimaging-informed multimedia analysis. For example, Hu et al. (2015) proposed a HAFNI-based fMRI decoding

Table 15.3 Ratio of Distribution Percentage of THFRs on Gyri vs. That on Sulci in All Subjects (the Ratio Is Represented as Mean \pm Standard Deviation)

	Emotion	Gambling	Language	Motor	Rational	Social	WM
Ratio	2.22 \pm 1.09	3.14 \pm 3.87	2.63 \pm 2.07	2.95 \pm 2.47	3.38 \pm 4.29	2.50 \pm 1.32	2.76 \pm 1.59
p-Value	9.48E -22	9.60E -19	2.98E -20	1.56E -19	1.49E -17	8.25E -22	8.29E -22

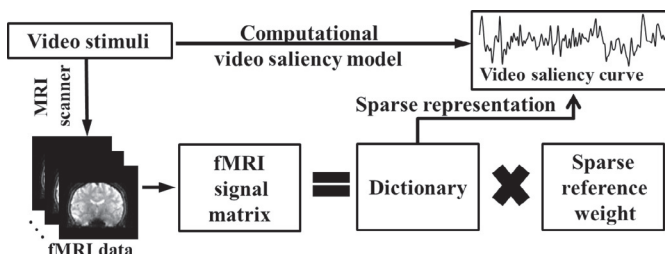


FIG. 15.10

The computational framework of the HAFNI-based fMRI decoding model to decode the bottom-up visual saliency in video streams based on whole-brain natural stimulus fMRI signals.

model to decode the bottom-up visual saliency in video streams using recorded whole-brain natural stimulus fMRI signals. As illustrated in Fig. 15.10, the video stimuli are analyzed based on a computational video saliency model to obtain the video saliency curves. Meanwhile, the whole-brain natural stimulus fMRI signals under the video stimuli are decomposed into the dictionary and sparse reference weight matrix via the HAFNI framework. The learned dictionary components are then adopted to sparsely represent the video saliency curves. The experimental results show that the learned dictionary atoms of whole-brain fMRI signals can well decode the temporal visual saliency information in a naturalistic video stream, indicating that HAFNI-based sparse representation of brain activities measured by fMRI may benefit the multimedia content analysis field (Hu et al., 2015).

15.4 HAFNI-BASED NEW METHODS

As mentioned above, HAFNI is a pure data-driven approach. Recently, there has been increasing interest in introducing novel methodology or integrating brain science domain knowledge into the HAFNI framework, and the results are promising. For example, Zhao et al. (2015) proposed a novel supervised dictionary learning and sparse representation framework of tfMRI data for concurrent functional brain network inference. As illustrated in Fig. 15.11, the basic idea is to predefine the task stimulus curves in tfMRI data as the fixed model-driven dictionary atoms, and

merely optimize the other data-driven dictionary atoms. Specifically, the whole-brain tfMRI signals of one subject are firstly aggregated into a signal matrix. Then the supervised dictionary learning and sparse representation are performed to decompose the signal matrix into a dictionary matrix and a sparse reference weight matrix. In contrast to merely data-driven conventional dictionary learning, a constant part of dictionary atoms is defined as the model-driven task stimulus curves, and only the other dictionary atoms are optimized during dictionary learning (Fig. 15.11b). As a result, the part of sparse reference weight matrix which corresponds to the constant model-driven dictionary atoms represents the identified model-driven task-evoked functional networks. The other part of the sparse reference weight matrix represents the identified data-driven functional networks, including ICNs. This model-driven and data-driven integrated approach is effective and efficient in identifying both task-evoked networks and ICNs in all seven tfMRI datasets in HCP (Zhao et al., 2015).

A second example is the group-wise sparse representation of fMRI data of multiple groups of subjects (Lv et al., 2015c), which has already been illustrated in Fig. 15.6. Instead of the conventional sparse representation of fMRI signals for one single subject, the group-wise sparse representation learns a common dictionary matrix from the aggregated signal matrix of multiple groups of subjects. As illustrated in Fig. 15.7, this approach has the potential to be applied to clinical data

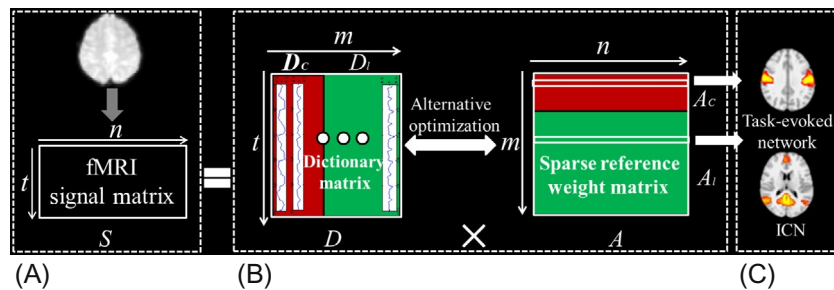


FIG. 15.11

The computational framework of supervised dictionary learning and sparse representation of tfMRI data for identification of concurrent functional brain networks. (A) FMRI signal matrix S aggregated from the whole-brain fMRI signals of one subject. t is the fMRI time point and n is the voxel number. (B) The learned dictionary D and sparse reference weight matrix A based on the supervised dictionary learning and sparse representation. m is the number of dictionary atoms. D_c refers to the predefined dictionary atoms based on model-driven task stimulus curves and is kept unchanged. D_l denotes the other part of dictionary atoms which is optimized during dictionary learning. A_c , which corresponds to D_c , represents the identified model-driven task-evoked functional networks. A_l , which corresponds to D_l , represents other identified data-driven functional networks including ICNs. (C) Two examples of identified model-driven task-evoked functional network and data-driven ICNs.

which includes multiple groups (eg, normal control and diseased groups) to identify a collection of functional brain networks/regions which are possibly affected by the disease (Lv et al., 2015c). A third example is a two-stage dictionary learning and sparse representation framework to differentiate the tfMRI and rsfMRI data (Zhang et al., 2016). The core idea is to perform dictionary learning and sparse representation of whole-brain fMRI signals twice. In the first stage, the HAFNI framework is applied to the whole-brain tfMRI or rsfMRI signals of each subject. In the second stage, all learned dictionary matrices of tfMRI and rsfMRI from the first stage are aggregated into one matrix and the matrix is further decomposed into a dictionary matrix and a sparse reference weight matrix (Zhang et al., 2016). This approach is capable of identifying the distinctive and descriptive dictionary atoms within the dictionary matrix in the second stage, and is able to effectively discriminate tfMRI and rsfMRI signals (Zhang et al., 2016).

15.5 FUTURE DIRECTIONS OF HAFNI APPLICATIONS

The HAFNI framework can be enhanced in the future in the following aspects. First, advanced algorithms such as signal sampling strategies (Ge et al., 2015) may be introduced and integrated to speed up the dictionary learning and sparse representation procedure. Second, our recently developed HAFNI-Enabled Largescale Platform for Neuroimaging Informatics (HELPNI) (Makkie et al., 2015) or Hadoop/SPARK-based systems can be implemented to handle fMRI “big data.” Third, the HAFNI framework can be adopted to analyze brain dynamics and to establish functional dynamic HAFNI. Finally, HAFNI can also be adopted to identify network-based neuroimaging biomarkers to characterize, subtype, and diagnose other neurological/psychiatric disorders (eg, autism, schizophrenia, post-traumatic stress disorder, etc.).

ACKNOWLEDGMENTS

The HAFNI framework and its applications summarized in this chapter are based on the works of CAID lab members (<http://caid.cs.uga.edu/>) and their collaborators. We would like to thank all of them.

REFERENCES

- Andersen, A.H., Gash, D.M., Avison, M.J., 1999. Principal component analysis of the dynamic response measured by fMRI: a generalized linear systems framework. *Magn. Reson. Imaging* 17 (6), 795–815.
- Anderson, M.L., Kinnison, J., Pessoa, L., 2013. Describing functional diversity of brain regions and brain networks. *NeuroImage* 73, 50–58.

- Bandettini, P.A., Jesmanowicz, A., Wong, E.C., Hyde, J.S., 1993. Processing strategies for time-course data sets in functional MRI of the human brain. *Magn. Reson. Med.* 30 (2), 161–173.
- Biswal, B.B., Yetkin, F.Z., Haughton, V.M., Hyde, J.S., 1995. Functional connectivity in the motor cortex of resting human brain using echo-planar MRI. *Magn. Reson. Med.* 34, 537–541.
- Bullmore, E., Fadili, J., Breakspear, M., Salvador, R., Suckling, J., Brammer, M., 2003. Wavelets and statistical analysis of functional magnetic resonance images of the human brain. *Stat. Meth. Med. Res.* 12 (5), 375–399.
- Calhoun, V.D., Adali, T., 2006. ‘Unmixing’ functional magnetic resonance imaging with independent component analysis. *IEEE Eng. Med. Biol. Mag.* 25 (2), 79–90.
- Chang, C.C., Lin, C.J., 2011. LIBSVM: a library for support vector machines. *ACM Trans. Intell. Syst. Technol.* 2 (3), 27.
- Cohen, A.L., Fair, D.A., Dosenbach, N.U.F., Miezin, F.M., Dierker, D., Van Essen, D.C., Schlaggar, B.L., Petersen, S.E., 2008. Defining functional areas in individual human brains using resting functional connectivity MRI. *NeuroImage* 41, 45–57.
- Deng, F., Zhu, D., Lv, J., Guo, L., Liu, T., 2012. fMRI signal analysis using empirical mean curve decomposition. *IEEE Trans. Biomed. Eng.* 60 (1), 42–54.
- Descombes, X., Kruggel, F., von Cramon, D.Y., 1998. fMRI signal restoration using a spatio-temporal Markov random field preserving transitions. *NeuroImage* 8 (4), 340–349.
- DuBois Bowman, F., Caffo, B., Bassett, S.S., Kilts, C., 2008. Bayesian hierarchical framework for spatial modeling of fMRI data. *NeuroImage* 39, 146–156.
- Duncan, J., 2010. The multiple-demand (MD) system of the primate brain: mental programs for intelligent behaviour. *Trends Cogn. Sci.* 14 (4), 172–179.
- Fedorenko, E., Duncan, J., Kanwisher, N., 2013. Broad domain generality in focal regions of frontal and parietal cortex. *Proc. Natl. Acad. Sci. USA* 110 (41), 16616–16621.
- Fox, M.D., Raichle, M.E., 2007. Spontaneous fluctuations in brain activity observed with functional magnetic resonance imaging. *Nat. Rev. Neurosci.* 8 (9), 700–711.
- Friston, K.J., 2009. Modalities, modes, and models in functional neuroimaging. *Science* 326, 399–403.
- Friston, K.J., Holmes, A.P., Worsley, K.J., Poline, J.P., Frith, C.C., Frackowiak, R.S.J., 1994. Statistical parametric maps in functional imaging: a general linear approach. *Hum. Brain Map.* 2 (4), 189–210.
- Ge, B., Makkie, M., Wang, J., Zhao, S., Jiang, X., Li, X., Lv, J., Zhang, S., Zhang, W., Han, J., Guo, L., Liu, T., 2015. Signal sampling for efficient sparse representation of resting state fMRI data. *Brain Imaging Behav.* In press. Epub ahead of print. <http://dx.doi.org/10.1007/s11682-015-9487-0>.
- Hall, M.A., Smith, L.A., 1999. Feature selection for machine learning: comparing a correlation-based filter approach to the wrapper. In: In FLAIRS Conference 1999, pp. 235–239.
- Hartvig, N.V., Jensen, J.L., 2000. Spatial mixture modeling of fMRI data. *Hum. Brain Map.* 11 (4), 233–248.
- Hu, X., Lv, C., Cheng, G., Lv, J., Guo, L., Han, J., Liu, T., 2015. Sparsity constrained fMRI decoding of visual saliency in naturalistic video streams. *IEEE Trans. Auton. Ment. Dev.* 7 (2), 65–75.
- Jiang, X., Zhang, X., Zhu, D., 2014. Intrinsic functional component analysis via sparse representation on Alzheimer’s disease neuroimaging initiative database. *Brain Connect.* 4 (8), 575–86.

- Jiang, X., Li, X., Lv, J., Zhang, T., Zhang, S., Guo, L., Liu, T., 2015. Sparse representation of HCP grayordinate data reveals novel functional architecture of cerebral cortex. *Hum. Brain Map.* 36 (12), 5301–5319.
- Kanwisher, N., 2010. Functional specificity in the human brain: a window into the functional architecture of the mind. *Proc. Natl. Acad. Sci. USA* 107 (25), 11163–11170.
- Krekelberg, B., Boynton, G.M., Van Wezel, R.J., 2006. Adaptation: from single cells to bold signals. *Trends Neurosci.* 29 (5), 250–256.
- Logothetis, N.K., 2008. What we can do and what we cannot do with fMRI. *Nature* 453, 869–878.
- Lv, J., Jiang, X., Li, X., Zhu, D., Chen, H., Zhang, T., Zhang, S., Hu, X., Han, J., Huang, H., Zhang, J., Guo, L., Liu, T., 2015a. Sparse representation of whole-brain fMRI signals for identification of functional networks. *Med. Image Anal.* 20 (1), 112–134.
- Lv, J., Jiang, X., Li, X., Zhu, D., Zhang, S., Zhao, S., Chen, H., Zhang, T., Hu, X., Han, J., Ye, J., Guo, L., Liu, T., 2015b. Holistic atlases of functional networks and interactions reveal reciprocal organizational architecture of cortical function. *IEEE Trans. Biomed. Eng.* 62 (4), 1120–1131.
- Lv, J., Jiang, X., Li, X., Zhu, D., Zhao, S., Zhang, T., Hu, X., Han, J., Guo, L., Li, Z., Coles, C., Hu, X., Liu, T., 2015c. Assessing effects of prenatal alcohol exposure using group-wise sparse representation of fMRI data. *Psychiatr. Res. Neuroimaging* 233 (2), 254–68.
- Mairal, J., Bach, F., Ponce, J., Sapiro, G., 2010. Online learning for matrix factorization and sparse coding. *J. Mach. Learn. Res.* 11, 19–60.
- Makkie, M., Zhao, S., Jiang, X., Lv, J., Zhao, Y., Ge, B., Li, X., Han, J., Liu, T., 2015. HAFNI-enabled largescale platform for neuroimaging informatics (HELPNI). *Brain Inform. form.* 2 (4), 1–17.
- McKeown, M.J., Jung, T.P., Makeig, S., Brown, G., Kindermann, S.S., Lee, T.W., Sejnowski, T.J., 1998. Spatially independent activity patterns in functional MRI data during the stroop color-naming task. *Proc. Natl. Acad. Sci. USA* 95 (3), 803.
- McKeown, M.J., Hansen, L.K., Sejnowski, T.J., 2003. Independent component analysis of functional MRI: what is signal and what is noise? *Curr. Opin. Neurobiol.* 13 (5), 620–629.
- Ogawa, S., Lee, T.M., Kay, A.R., Tank, D.W., 1990a. Brain magnetic resonance imaging with contrast dependent on blood oxygenation. *Proc. Natl. Acad. Sci. USA* 87 (24), 9868–9872.
- Ogawa, S., Lee, T.M., Nayak, A.S., Glynn, P., 1990b. Oxygenation-sensitive contrast in magnetic resonance image of rodent brain at high magnetic fields. *Magn. Reson. Med.* 14, 68–78.
- Pessoa, L., 2012. Beyond brain regions: network perspective of cognition-emotion interactions. *Behav. Brain Sci.* 35 (03), 158–159.
- Petersen, R.C., Stevens, J.C., Ganguli, M., Tangalos, E.G., Cummings, J.L., DeKosky, S.T., 2001. Practice parameter: early detection of dementia: mild cognitive impairment (an evidence-based review). report of the quality standards subcommittee of the American Academy of Neurology. *Neurology* 56, 1133–1142.
- Rakic, P., 1988. Specification of cerebral cortical areas. *Science* 241, 170–176.
- Shimizu, Y., Barth, M., Windischberger, C., Moser, E., Thurner, S., 2004. Wavelet-based multifractal analysis of fMRI time series. *NeuroImage* 22, 1195–1202.
- Smith, S.M., Fox, P.T., Miller, K.L., Glahn, D.C., Fox, P.M., Mackay, C.E., Filippini, N., Watkins, K.E., Torod, R., Laird, A.R., Beckmann, C.F., 2009. Correspondence of the

- brain's functional architecture during activation and rest. *Proc. Natl. Acad. Sci. USA* 106 (31), 13040–13045.
- Smith, S.M., Andersson, J., Auerbach, E.J., Beckmann, C.F., Bijsterbosch, J., Douaud, G., Duff, E., Feinberg, D.A., Griffanti, L., Harms, M.P., Kelly, M., Laumann, T., Miller, K.L., Moeller, S., Petersen, S., Power, J., Salimi-Khorshidi, G., Snyder, A.Z., Vu, A.T., Woolrich, M.W., Xu, J., Yacoub, E., Urbil, K., Van Essen, D.C., Glasser, M.F., 2013. Resting-state fMRI in the human connectome project. *NeuroImage* 80 (15), 144–168.
- Thies, W., Bleiler, L., 2013. Alzheimer's disease facts and figures. *Alzheimer's Dementia* 9 (2), 208–45.
- van den Heuvel, V., Pol, H.H., 2010. Exploring the brain network: a review on resting-state fMRI functional connectivity. *Eur. Neuropsychopharmacol.* 20 (8), 519–534.
- Van Den Heuvel, M., Mandl, R., Luigjes, J., Hulshoff Pol, H., 2008. Microstructural organization of the cingulum tract and the level of default mode functional connectivity. *J. Neurosci.* 28, 10844–51.
- Van Essen, D.C., Smith, S.M., Barch, D.M., Behrens, T.E., Yacoub, E., Ugurbil, K., WU-Minn HCP Consortium, 2013. The Wu-Minn human connectome project: an overview. *NeuroImage* 80, 62–79.
- Varoquaux, G., Schwartz, Y., Pinel, P., Thirion, B., Wells, W.M., Joshi, S., Pohl, K., 2013. Co-hort-level brain mapping: learning cognitive atoms to single out specialized regions. In: IPMI-Information Processing in Medical Imaging, LNCS vol. 7917. Springer, Heidelberg, pp. 438–449.
- Wagenmakers, E.J., 2015. An Introduction to Model-Based Cognitive Neuroscience. Forstmann, B.U. (Ed.). Springer, New York.
- Woolrich, M., Ripley, B., Brady, J., Smith, S., 2001. Temporal autocorrelation in univariate linear modelling of fMRI data. *NeuroImage* 14 (6), 1370–1386.
- Worsley, K.J., 1997. An overview and some new developments in the statistical analysis of pet and fMRI data. *Hum. Brain Map.* 5 (4), 254–258.
- Zhang, S., Li, X., Lv, J., Jiang, X., Guo, L., Liu, T., 2016. Characterizing and differentiating task-based and resting state fMRI signals via two-stage sparse representations. *Brain Imaging Behav.* 10 (1), 21–32.
- Zhao, S., J., H., Lv, J., Jiang, X., Hu, X., Zhao, Y., Ge, B., Guo, L., Liu, T., 2015. Supervised dictionary learning for inferring concurrent brain networks. *IEEE Trans. Med. Imaging* 34 (10), 2036–2045.